Dalton Transactions

ROYAL SOCIETY OF CHEMISTRY

PAPER

View Article Online
View Journal | View Issue

Cite this: *Dalton Trans.*, 2025, **54**, 10234

Electron deficient β-trisubstituted porphyrins: synthesis, structural, spectral, and electrochemical studies and their intensity-dependent third-order nonlinear optical properties†

Reena Jangra,‡[a] Amritha J. Nair,‡[a] Albin Kuriakose,[b] Jitendra Nath Acharyya,[b] G. Vijaya Prakash *[b] and Muniappan Sankar *[a]

A series of electron-deficient β-trisubstituted 12-nitro-5,10,15,20-tetraphenyl-2,3-bis(trifluoromethyl) porphyrins, abbreviated as $H_2TPP(NO_2)(CF_3)_2$, and their metal complexes $MTPP(NO_2)(CF_3)_2$ (where M = Co^{II}, Ni^{II}, Cu^{II}, and Zn^{II}) have been prepared and characterised by various spectroscopic techniques. Single crystal X-ray analysis revealed the *saddle*-shaped configuration of $CoTPP(NO_2)(CF_3)_2$, $NiTPP(NO_2)(CF_3)_2$ and $CuTPP(NO_2)(CF_3)_2$ with the average deviation of the 24 core atoms from the mean porphyrin plane (Δ24) ranging from ±0.492 to ±0.499 Å and the average displacement of β-pyrrole carbons from the porphyrin mean plane (ΔC_β) ranging from ±0.926 to ±1.005 Å. $H_2TPP(NO_2)(CF_3)_2$ exhibited a 28 nm red shift in the B-band and a 102 nm red shift in the longest Q-band ($Q_x(0,0)$) as compared to H_2TPP. In ^1H NMR, the inner imino protons of $H_2TPP(NO_2)(CF_3)_2$ were observed at −1.72 ppm, which is significantly downfield shifted compared to H_2TPP. The first ring reduction potential of $MTPP(NO_2)(CF_3)_2$ (M = 2H, Co^{II}, Ni^{II}, Cu^{II}, and Zn^{II}) is positively shifted by 280–620 mV compared to their corresponding MTPPs. Notably, it is observed that the synthesized $MTPP(NO_2)(CF_3)_2$ porphyrins are readily reduced compared to their MTPPs. Intensity-dependent third-order nonlinear optical property studies demonstrated that the synthesized asymmetric β-substituted electron-deficient porphyrins exhibit significant two-photon absorption coefficients (β = 0.04–8.10 × 10^{-10} m W^{-1}) and two-photon absorption cross-section values (σ_{2PA} = 0.02–1.67 × 10^6 GM). Additionally, the materials exhibit self-defocusing negative nonlinear refraction (n_2 = (−) 1.08–40.27 × 10^{-17} m^2 W^{-1}). The extracted NLO data suggest the potential of the investigated porphyrins for future optoelectronic and advanced material applications.

Received 14th March 2025,
Accepted 21st May 2025

DOI: 10.1039/d5dt00618j

rsc.li/dalton

Introduction

The potential application of nonlinear optical (NLO) materials in optical computing, image processing, optical fibers, optical switching, optical limiting, optical communication, and optical data storage has garnered significant research attention in this field.[1–11] The development of novel NLO materials exhibiting strong NLO responses and high stability is urgently required to meet the demands of various applications across different fields. In this regard, porphyrins emerge as particularly promising candidates for nonlinear optical properties.[12,13] This is attributed to their highly delocalized aromatic π-electron systems, substantial stability, conformational flexibility, and potential for versatile structural modifications.[14–34] However, additional factors such as the position, nature, and polarizability of the rings or nature of the substituents, intramolecular and transition dipole moments, and the orthogonality of the substituents, molecular dihedral angle, and oxidation state of the metal ions can also significantly enhance the NLO response.[35] These features collectively improve their suitability for tuning NLO responses. Ongoing research in developing NLO materials has yielded diverse porphyrin structures. These structures include push–pull porphyrins,[36] symmetric[15,17,18] and asymmetric porphyrins,[19–21,37] porphyrin oligomers,[22–24] expanded porphyrins[28] and porphyrin arrays.[29–32] The third-order NLO properties of porphyrin derivatives can be modulated through metal complexation,[38,39] π-conjugation, and functionalization.[40,41] In contrast, the second-order NLO pro-

[a]*Department of Chemistry, Indian Institute of Technology Roorkee, Roorkee-247667, India. E-mail: m.sankar@cy.iitr.ac.in*
[b]*Nanophotonics Lab, Department of Physics, Indian Institute of Technology Delhi, New Delhi-110016, India. E-mail: prakash@physics.iitd.ac.in*

†Electronic supplementary information (ESI) available. CCDC 2389047–2389049. For ESI and crystallographic data in CIF or other electronic format see DOI: https://doi.org/10.1039/d5dt00618j

‡These authors contributed equally.

perties of porphyrin and its derivatives have been infrequently studied, primarily due to the centrosymmetric nature of pristine porphyrins.[42,43] However, by disturbing the centrosymmetry, porphyrin derivatives could exhibit significant NLO responses; keeping this in mind, our research group is currently focused on synthesizing unsymmetrical porphyrins and corroles for NLO applications. In 2017, Yadav and co-workers synthesized push–pull *trans*-A_2B-corroles and studied their femtosecond third-order NLO properties.[44] In 2020, Rathi and co-workers prepared unsymmetrical push–pull porphyrins and characterized their effect on metal insertion in ultrafast NLO materials.[45] In 2021, Kumar and coworkers studied the strong two-photon absorption of *meso*-functionalized *trans*-A_2BC porphyrins.[46] In 2022, Rohal and co-workers synthesized unsymmetrical *β*-dicyanovinyl appended push–pull porphyrins as promising two-photon absorbers, and *β*-tetracyanobutadiene appended porphyrins as cost-effective optical limiters.[47,48] Bulbul and co-workers synthesized unsymmetrically *β*-functionalized *π*-extended porphyrins as efficient two-photon absorbers.[49] Yadav and co-workers studied ultrafast dynamics and strong two-photon absorbers of nonplanar *β*-functionalized push–pull copper corroles with mixed substituted patterns.[50] In 2023, Kumari and co-workers prepared a push–pull octaphenylporphyrin with different substituted patterns and characterized its ultrafast dynamics and NLO studies.[51] In 2024, Rohal and co-workers synthesized electron-deficient, nonplanar *β*-heptasubstituted porphyrin derivatives that exhibit an interesting three-photon absorption phenomenon.[52] In 2024, Bulbul and coworkers synthesized highly substituted Ni(II) porphyrins and *meso*-*β* monofused porphyrins and explored their third-order nonlinear optical properties.[53,54] Recently, Bulbul and coworkers synthesized *meso*-*β*, *β*–*β*′-trifused porphyrins and studied their femtosecond third-order nonlinear optical properties.[55]

Research on unsymmetrical porphyrins has predominantly focused on push–pull porphyrins, with limited studies on electron-deficient unsymmetrical porphyrins due to the challenges in their synthesis. However, unsymmetrically electron-deficient antipodal *β*-trisubstituted porphyrins have shown distinct electronic and photophysical properties, suggesting significant potential for broader future applications. Herein, the present work illustrates the synthesis of unsymmetrically electron-deficient *β*-trisubstituted porphyrins in good yields, characterized by different spectroscopic techniques and single crystal XRD, and explores their intensity-dependent third-order NLO properties.

Results and discussion

Synthesis and characterization

A series of electron-deficient *β*-trisubstituted 12-nitro-5,10,15,20-tetraphenyl-2,3-bis(trifluoromethyl)porphyrins ($H_2TPP(NO_2)(CF_3)_2$) and their metal complexes $MTPP(NO_2)(CF_3)_2$ (M = Co^{II}, Ni^{II}, Cu^{II} and Zn^{II}) were synthesized (see Chart 1) and thoroughly characterized using various spectroscopic techniques including UV-vis, fluorescence, and NMR spectroscopy, elemental analysis, single crystal X-ray analysis, and matrix-assisted laser desorption ionization time-of-flight (MALDI-TOF) mass spectrometry. Following established literature procedures, $H_2TPP(NO_2)Br_2$ and its copper complex were prepared.[56] The copper complex $CuTPP(NO_2)Br_2$ was charged with Chen's reagent ($FSO_2CF_2CO_2CH_3$) in the presence of a palladium catalyst (Pd(0)) and CuI as a co-catalyst, resulting in the formation of $CuTPP(NO_2)(CF_3)_2$ with a 65% conversion. The $CuTPP(NO_2)(CF_3)_2$ complex was demetallated using H_2SO_4, followed by remetallation with various metal salts, including Co^{II}, Ni^{II}, and Zn^{II} (see Scheme 1).

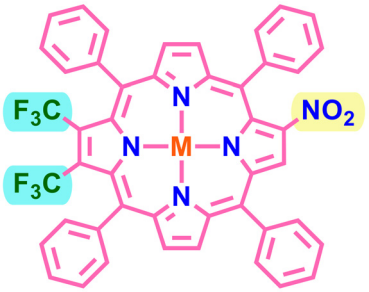

$H_2TPP(NO_2)(CF_3)_2$, (55 %)
$CoTPP(NO_2)(CF_3)_2$, (78 %)
$NiTPP(NO_2)(CF_3)_2$, (63 %)
$CuTPP(NO_2)(CF_3)_2$, (65 %)
$ZnTPP(NO_2)(CF_3)_2$, (78 %)

Chart 1 Molecular structure of electron-deficient *β*-trisubstituted porphyrins.

Single crystal X-ray diffraction analysis

Single crystal X-ray diffraction interpretation determined the exact spatial configuration and connectivity of trifluoromethyl

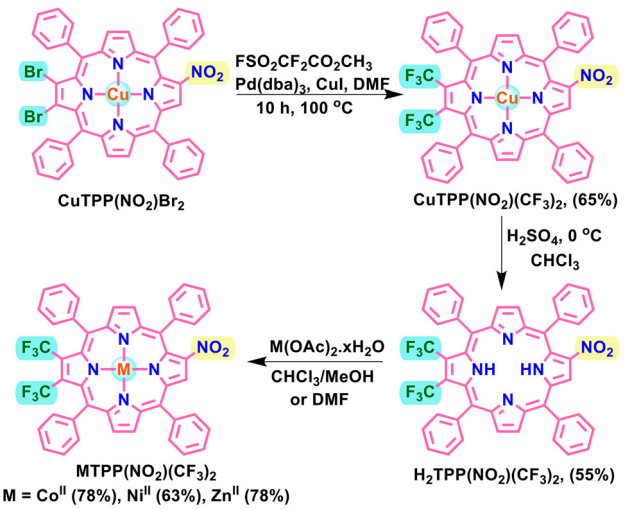

Scheme 1 Synthetic scheme for $MTPP(NO_2)(CF_3)_2$.

(CF_3) substituents at the pyrrolic carbons of porphyrins. The crystallization process of $CoTPP(NO_2)(CF_3)_2$, $NiTPP(NO_2)(CF_3)_2$, and $CuTPP(NO_2)(CF_3)_2$ described in this study involved the slow diffusion of hexane into a saturated solution of porphyrins in $CHCl_3$ at ambient temperature. The displacement of porphyrin 24 core atoms from the mean plane is shown in Fig. S1 in the ESI.† The crystallographic data, average bond lengths and angles of $CoTPP(NO_2)(CF_3)_2$, $NiTPP(NO_2)(CF_3)_2$, and $CuTPP(NO_2)(CF_3)_2$ are presented in Tables S1 and S2, respectively, in the ESI.† The ORTEP structures (top and side views) of $CoTPP(NO_2)(CF_3)_2$, $NiTPP(NO_2)(CF_3)_2$, and $CuTPP(NO_2)(CF_3)_2$ are shown in Fig. 1. $CoTPP(NO_2)(CF_3)_2$ and $CuTPP(NO_2)(CF_3)_2$ are crystallized in a *monoclinic* crystal system with a $P2_1/c$ space group, whereas $NiTPP(NO_2)(CF_3)_2$ is crystallized in the *triclinic* system with a $P\bar{1}$ space group. The single crystal X-ray analysis revealed the *saddle*-shaped configuration of all three porphyrins, with a mean plane deviation of 24 atoms (Δ24) ranging from ±0.492 to ±0.499 Å from the reference plane, although the deviation of β-carbon atoms (ΔC_β) was found to be in the range of ±0.926–±1.005 Å (see Fig. S1 in the ESI†), which is considerably higher than those reported for the published structures, $H_2TPP(CF_3)_2$, $NiTPP(NO_2)(Ph)_2$(pyridine), $ZnTPP(NO_2)(PE)_2(CH_3OH)$, $ZnTPP(NO_2)Br_2(CH_3OH)$ and $H_2TPP(NO_2)(Th)_2$ (Δ24 = ±0.061–±0.377 Å and ΔC_β = ±0.072–±0.750 Å).[56,57]

The nonplanarity of the porphyrin macrocycle is attributed to steric repulsion among the peripheral substituents, which necessitates strain release through adjustments in bond lengths and angles. Specifically, the C–C bond distance between the β-pyrrole carbon atoms (C_β–C_β bond lengths) bearing three β-substituents is longer than the $C_{\beta'}$–$C_{\beta'}$ distances, where the antipodal pyrroles are unsubstituted (see Table S2 in the ESI†). Notably, the N–M–N and N′–M′–N′ angles, ranging from 169.37° to 174.41°, deviate from 180°, signifying the nonplanar conformation of the M–$(N)_4$ core. Density functional theory (DFT) was employed for the free base and other metal complexes to carry out the complete geometry optimization.

Electronic spectral studies

The optical absorption properties of electron-deficient β-functionalized $MTPP(NO_2)(CF_3)_2$ (M = 2H, Co^{II}, Ni^{II}, Cu^{II}, and Zn^{II}) porphyrins were investigated in CH_2Cl_2 at 298 K. The electronic absorption spectra of porphyrin macrocycles are significantly influenced by the nature of the core metal ions, the presence of peripheral substituents, the shape of the molecule, and the extent of π-conjugation. The UV-visible absorption spectra of the presented porphyrins are shown in Fig. 2(a). The nonplanar conformation of the macrocycle is known to induce a distinctive red shift in their optical absorption properties.[58–60] Table 1 lists the optical absorption spectral data of all the presented porphyrins. $H_2TPP(NO_2)(CF_3)_2$ exhibited a 9 nm red shift in the B-band and a 67 nm red shift in the longest Q-band ($Q_x(0,0)$) as compared to $H_2TPP(NO_2)Br_2$, which can be attributed to the more electron-accepting effect of trifluoromethyl groups functionalized at the β-position of the pyrrole unit and the nonplanar conformation of the synthesized porphyrins, as demonstrated by the DFT calculations. $MTPP(NO_2)(CF_3)_2$, M = Co^{II}, Ni^{II}, Cu^{II}, and Zn^{II}, exhibited a 6–9 nm hypsochromic shift in the B-band as compared to $H_2TPP(NO_2)(CF_3)_2$, because of the stabilization of the highest occupied molecular orbital (HOMO) after insertion of metal. $H_2TPP(NO_2)(CF_3)_2$ exhibited a 28 nm bathochromic shift in the Soret band and a 105 nm red shift in the longest Q-band ($Q_x(0,0)$) as compared to H_2TPP.[61] This phenomenon is likely attributable to the conjugative or inductive interactions of the substituents with the π-system, as well as the nonplanarity of the porphyrin macrocycle, as demonstrated by the DFT calculations. $H_2TPP(NO_2)(CF_3)_2$ showed a 19 nm red shift in the B-band and an 86 nm red shift in the longest Q-band ($Q_x(0,0)$) as compared to H_2TPP

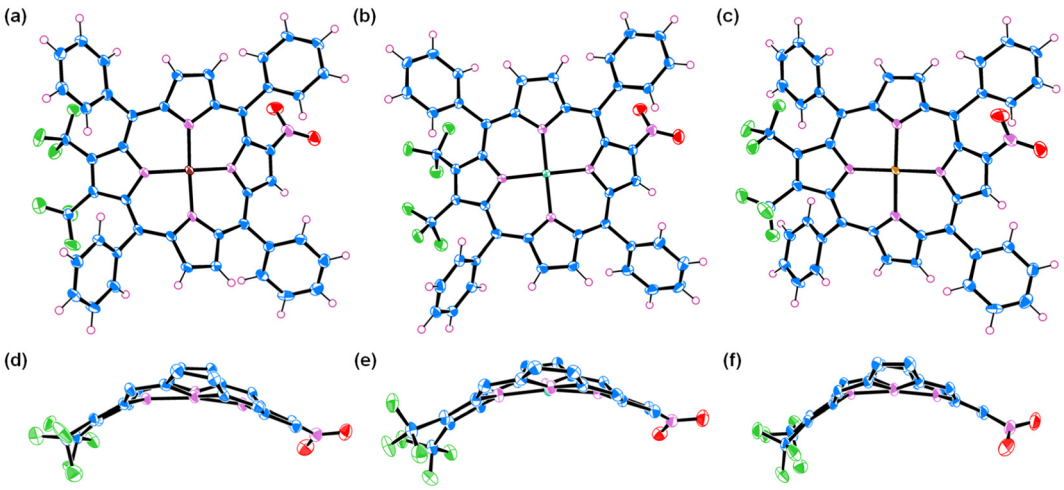

Fig. 1 ORTEP diagrams showing top (upper) and side views (lower) of $CoTPP(NO_2)(CF_3)_2$ (a and d), $NiTPP(NO_2)(CF_3)_2$ (b and e) and $CuTPP(NO_2)(CF_3)_2$ (c and f). Solvates are omitted for clarity, and the *meso*-phenyls are removed for clarity in the side views (d–f). Color codes: C (slate blue), N (orchid), O (red), H (violet-red), F (lime green), Co (brown), Ni (orange), and Cu (cool copper).

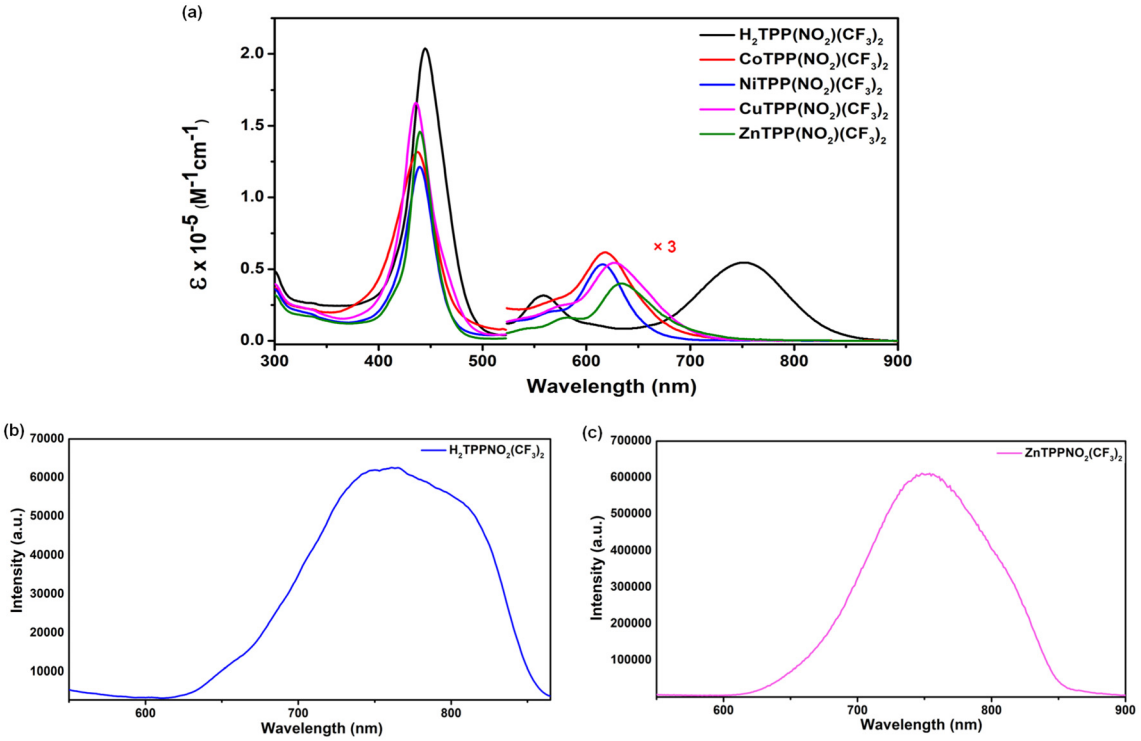

Fig. 2 (a) Electronic absorption spectra of MTPP$(NO_2)(CF_3)_2$ in CH_2Cl_2 at 298 K. Fluorescence spectra of (b) $H_2TPP(NO_2)(CF_3)_2$ and (c) $ZnTPP(NO_2)(CF_3)_2$ in CH_2Cl_2 at 298 K.

Table 1 Electronic spectral data of the synthesized porphyrins in CH_2Cl_2 at 298 K[a]

Porphyrins	λ_{abs}, nm	λ_{em}, nm	ϕ_f
$H_2TPP(NO_2)(CF_3)_2$	445 (204), 557 (10), 750 (18)	766	0.11
$CoTPP(NO_2)(CF_3)_2$	437 (132), 617 (20)		
$NiTPP(NO_2)(CF_3)_2$	439 (121), 614 (18)		
$CuTPP(NO_2)(CF_3)_2$	436 (166), 628 (18)		
$ZnTPP(NO_2)(CF_3)_2$	439 (145), 633 (13)	752	0.034

[a] Values in parentheses refer to $\varepsilon \times 10^{-3}$ (M^{-1} cm^{-1}).

(NO_2).[56] $H_2TPP(NO_2)(CF_3)_2$ exhibited a 1–6 nm bathochromic shift in the Soret band and 48–64 nm in the longest Q-band that resembled the mixed trisubstituted porphyrins as reported in the literature, which suggests the strongest electron-accepting effect of the trifluoromethyl group as compared to cyano, bromo, phenyl, 2-thienyl (Th) and phenylethynyl groups.[56] A similar type of disubstituted porphyrin ($H_2TPP(CF_3)_2$) reported in the literature showed a 6 nm blue shift in the B-band and a 42 nm blue shift in the longest Q-band compared to the synthesized $H_2TPP(NO_2)(CF_3)_2$, due to the presence of an electron-withdrawing nitro group.[57]

The synthesized free base and Zn^{II} β-functionalized porphyrins were characterized using fluorescence spectroscopy to investigate the influence of nonplanarity and substitutions. Fig. 2b and c show the steady-state emission spectra of the free base and Zn^{II} complex taken in CH_2Cl_2 at 298 K, and the emission data are tabulated in Table 1. $H_2TPP(NO_2)(CF_3)_2$ showed a 48 nm red-shifted emission compared to H_2TPP in CH_2Cl_2. $ZnTPP(NO_2)(CF_3)_2$ revealed a notable 103 nm red-shifted emission compared to ZnTPP. A significant red shift is observed due to the presence of electron-accepting nitro and trifluoromethyl groups. $H_2TPP(NO_2)(CF_3)_2$ and $ZnTPP(NO_2)(CF_3)_2$ showed qualitative quantum yields comparable to those of H_2TPP and ZnTPP.

NMR spectral studies and mass spectrometry

The ^1H NMR spectra of the synthesized porphyrins, MTPP$(NO_2)(CF_3)_2$ (where M = 2H, Ni^{II} and Zn^{II}), were obtained in $CDCl_3$ at 298 K. The ^1H NMR signals for all the synthesized porphyrins were attributed to *meso*-phenyl protons, β-pyrrole protons, and inner imino protons in the case of the free base. The integration of the proton signals is consistent with the synthesized porphyrin structures. Fig. S2–S4 in the ESI† show the ^1H NMR spectra of $H_2TPP(NO_2)(CF_3)_2$, $NiTPP(NO_2)(CF_3)_2$ and $ZnTPP(NO_2)(CF_3)_2$. A singlet peak at 8.85 ppm is observed for the synthesized free base porphyrin corresponding to the β-proton adjacent to the β-nitro group. The remaining four β-protons exhibited one doublet of triplet and one multiplet at 8.70 ppm and 8.60 ppm, respectively (see Fig. S2 in the ESI†). The *meso*-phenyl protons exhibit a multiplet between 7.76 and 8.28 ppm. The inner imino protons were observed at −1.72 ppm. Notably, it is observed that the resonance of inner imino protons is highly downfield shifted (0.81–0.93 ppm) as compared to the mixed trisubstituted porphyrins reported in

the literature, due to the more electron-accepting effect of the trifluoromethyl group and non-planar conformation.[56] The nonplanarity of the macrocycle induces broad features in the resonance of the imino protons, shifting them to the downfield region compared to those in planar porphyrins.[62,63] Similarly, Ni^{II} and Zn^{II} complexes showed analogous spectra to $H_2TPP(NO_2)(CF_3)_2$. The integration of all the proton signals corresponded well with the proposed structures.

^{19}F and ^{13}C NMR spectra of $ZnTPP(NO_2)(CF_3)_2$ are recorded in $CDCl_3$ and shown in Fig. S5 and S6, respectively, in the ESI.† In the ^{19}F NMR spectrum, $ZnTPP(NO_2)(CF_3)_2$ shows two peaks at −46.54 ppm (3F) and −46.70 ppm (3F). ^{13}C NMR spectra showed macrocycle signals ranging from 119.73 to 152.79 ppm.

All the synthesized porphyrins were characterized by MALDI-TOF mass spectrometry. All the mass spectra were recorded in positive ion mode using CH_2Cl_2 as a solvent at 298 K and are shown in Fig. S7–S11 in the ESI.†

DFT studies

To investigate the influence of substituents at the *β*-pyrrolic position of the porphyrin macrocycle and to validate the experimental results, we performed the optimization of the ground state geometries for the electron-deficient *β*-trisubstituted porphyrins $MTPP(NO_2)(CF_3)_2$, M = 2H, Co^{II}, Ni^{II}, Cu^{II}, and Zn^{II} in the gas phase using Gaussian 16 software. The calculations were performed with the B3LYP functional set and 6-31G basis set for the free base, while the LANL2DZ basis set was used for the metal complexes. The synthesized porphyrins' optimized geometry (top and side views) is shown in Fig. S12 in the ESI† and frontier molecular orbitals (FMOs) are shown in Fig. S13 in the ESI.† According to Gouterman's four orbital models, the highest occupied molecular orbitals (HOMOs) exhibit electron density contribution from *meso*-carbon and pyrrolic nitrogen, which corresponds to the a_{2u} type, whereas HOMO−1 exhibits electron density at pyrrolic carbons, which is classified as the a_{1u} type. The lowest occupied molecular orbitals (LUMOs) exhibited electron density at opposite substituted pyrrolic moieties, *meso*-carbons, and the nitro group, whereas LUMO−1 showed electron density at the opposite unsubstituted pyrrolic moieties, *meso*-carbons, and the nitro group. The calculated average bond lengths and angles are tabulated in Table S3 in the ESI.† The peripheral substituents may induce steric hindrance in the porphyrins, which can be alleviated by modifying the bond angles and lengths in the nonplanarity of the ring. Electron-accepting moieties increase the C_β–C_β and M–N bond lengths as compared to the $C_{\beta'}$–$C_{\beta'}$ and M–N′ bond lengths of the synthesized porphyrins $MTPP(NO_2)(CF_3)_2$, M = 2H, Co^{II}, Ni^{II}, Cu^{II}, and Zn^{II} (see Table S3 in the ESI†). The synthesized porphyrins exhibited a mean plane deviation of Δ24 atoms ranging from ±0.318 to ±0.768 Å, whereas the deviation of ΔC_β ranges from ±0.389 to ±0.875 Å. The theoretically calculated ground state dipole moment in the gas phase of the synthesized porphyrins ranges from 6.42 to 7.75 Debye (D) and is listed in Table S4 in the ESI.†

Electrochemical studies

The electrochemical redox potentials of the macrocyclic *π*-system are affected by the nature of the *β*-substituents, nonplanar conformation, and the core metal ions. To elucidate the combined effect of macrocyclic nonplanarity and the electron-accepting nature of the *β*-functionalized trifluoromethyl substituent, we investigated the electrochemical redox characteristics of the presented porphyrins in CH_2Cl_2 with 0.1 M $TBAPF_6$ as the supporting electrolyte at 298 K using cyclic voltammetry. Fig. 3 shows the cyclic voltammogram, and Table 2 lists the redox potential (*vs.* Ag/AgCl) data of all the synthesized porphyrins. The synthesized free base porphyrin, $H_2TPP(NO_2)(CF_3)_2$, exhibits three successive one-electron reversible oxidations and one two-electron reversible reduction, whereas $CoTPP(NO_2)(CF_3)_2$ undergoes three successive one-electron reversible oxidations and two one-electron reversible reductions. The first oxidation and reduction of Co^{II} correspond to the metal-centered redox activity, well-documented in the literature,[64,65] whereas the second and third oxidations correspond to the ring-centered redox activity. $NiTPP(NO_2)(CF_3)_2$ demonstrates one successive two-electron oxidation and two one-electron reductions. $CuTPP(NO_2)(CF_3)_2$ reveals two successive one-electron reversible oxidation and reduction peaks. In comparison, $ZnTPP(NO_2)(CF_3)_2$ exhibited two successive one-electron reversible oxidations and two close reduction processes merged to produce an average potential at −0.85 V (see Fig. 3).

The impact of the *β*-substituted trifluoromethyl group ($MTPP(NO_2)(CF_3)_2$) on the porphyrin macrocycle is characterized by comparing the first reduction potential peak with those of the corresponding $MTPP(NO_2)$ and MTPPs (see Table 2). It is observed that the first ring reduction potential of $MTPP(NO_2)(CF_3)_2$ is positively shifted by 190–350 mV and 280–680 mV compared to their corresponding $MTPP(NO_2)$ and

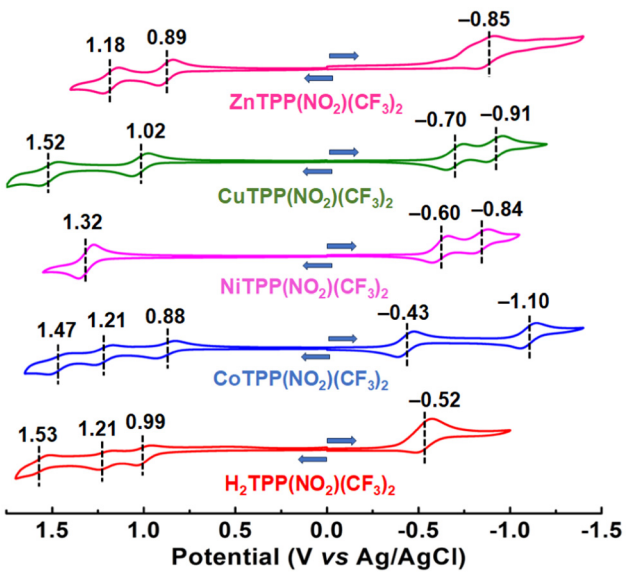

Fig. 3 Cyclic voltammograms (CVs) of all the synthesized porphyrins in CH_2Cl_2 at 298 K. Scan rate - 0.1 V sec^{-1}.

Table 2 Comparative electrochemical redox data (*vs.* Ag/AgCl) of the synthesized porphyrins ($MTPP(NO_2)(CF_3)_2$), with their parent porphyrins[a] MTPP and $MTPP(NO_2)$ in CH_2Cl_2 containing 0.1 M $TBAPF_6$ at 298 K

Porphyrins	Oxidation (V)			Reduction (V)			ΔE (V)
	I	II	III	I	II	III	
H_2TPP	1.00	1.34		−1.23	−1.54		2.23
$H_2TPP(NO)_2$	1.10	1.28		−0.87	−1.08		1.97
$H_2TPP(NO)_2(CF_3)_2$	**0.99**	**1.21**	**1.53**	**−0.52**			**1.51**
CoTPP	0.85	1.06	1.32	−0.86	−1.38		2.44
$CoTPP(NO)_2$	0.91	1.17	1.42	−0.66	−1.29	−1.89	2.46
$CoTPP(NO)_2(CF_3)_2$	**0.88**	**1.21**	**1.47**	**−0.43**	**−1.10**		**2.31**
NiTPP	1.02	1.32		−1.28	−1.72		2.30
$NiTPP(NO)_2$	1.18	1.31		−0.94	−1.21		2.12
$NiTPP(NO)_2(CF_3)_2$	**1.32**			**−0.60**	**−0.84**		**1.92**
CuTPP	0.97	1.35		−1.32	−1.71		2.29
$CuTPP(NO)_2$	1.07	1.44		−0.98	−1.23		2.05
$CuTPP(NO)_2(CF_3)_2$	**1.02**	**1.52**		**−0.70**	**−0.91**		**1.72**
ZnTPP	0.83	1.14		−1.36	−1.76		2.19
$ZnTPP(NO)_2$	0.91	1.21		−1.04	−1.19		1.95
$ZnTPP(NO)_2(CF_3)_2$	**0.89**	**1.18**		**−0.85**			**1.74**

[a] Electrochemical data of MTPP and $MTPP(NO_2)$ are taken from ref. 56.

MTPPs, respectively.[56] β-Substituents also influence the metal-centered redox potential properties; for instance, the first metal-centered reduction potential of $CoTPP(NO_2)(CF_3)_2$ is 230 mV and 430 mV anodically shifted compared to CoTPP (NO_2) and CoTPP, respectively (see Table 2).[56]

Notably, it is observed that the first ring reduction potential of $MTPP(NO_2)(CF_3)_2$ is 89–342 mV anodically shifted compared to the reported trisubstituted porphyrins $MTPP(NO_2)X_2$ (X = Br, Ph, PE and Th) in the literature.[56] However, among the $MTPP(NO_2)(CF_3)_2$, Cu^{II} and Zn^{II} complexes showed a cathodic shift. In contrast, Ni^{II} and Co^{II} complexes showed an anodic shift in the first ring reduction potential as compared to the corresponding $MTPP(NO_2)(CN)_2$.[56] Trisubstituted $MTPP(NO_2)(CF_3)_2$ (M = 2H, Co^{II}, Ni^{II}, Cu^{II}, and Zn^{II}), are readily reducible compared to related disubstituted porphyrins $MTPP(CF_3)_2$ (M = 2H, Co^{II}, Ni^{II}, Cu^{II}, and Zn^{II}) as reported in the literature,[57] due to the presence of the nitro group. Among all the synthesized porphyrins, $H_2TPP(NO_2)(CF_3)_2$ has shown a lower HOMO–LUMO gap (1.51 V). A remarkable reduction in the HOMO–LUMO energy gap of 0.72 V, 0.43 V and 0.36 V was observed in $H_2TPP(NO_2)(CF_3)_2$ compared to H_2TPP (2.23 V), $H_2TPP(NO_2)$ (1.97 V) and $H_2TPP(NO_2)Br_2$ (1.87 V), respectively.[56]

Intensity-dependent NLO studies

Investigating third-order nonlinear optical properties of different materials is essential for developing various nonlinear photonic device applications. When a high-intensity laser beam interacts with a material, the absorption and refraction coefficients of the materials change as functions of the intensity of the incident laser beam. The mathematical relationship that shows the variation in absorption and refraction coefficients with incident laser intensity is given by

$$\alpha(I) = \alpha_0 + \beta I \text{ and } n(I) = n_0 + n_2 I \quad (1)$$

where α_0 and n_0 are the linear absorption coefficient and refractive index of the material. Similarly, β, n_2 and I are the third-order nonlinear two-photon absorption (TPA) coefficient, nonlinear refractive index and incident laser intensity. The single Gaussian beam-based *Z*-scan technique is the most effective method for obtaining the third-order nonlinear optical properties of a material.[66] The single Gaussian beam *Z*-scan technique involves focusing a Gaussian laser beam on the sample using a convex lens. The laser beam that is transmitted through the sample is detected at each position as the sample is moved across the focal point. The nonlinear two-photon absorption coefficient is obtained using an open aperture (OA) *Z*-scan configuration in which the complete transmitted beam through the sample is collected using a photodetector. The nonlinear refraction property of the material is studied using the closed aperture (CA) *Z*-scan configuration, in which an aperture is placed before the collecting lenses. This straightforward single Gaussian beam *Z*-scan technique allows the estimation of the magnitude and sign of the third-order nonlinear coefficients, including the nonlinear refractive index (n_2), nonlinear absorption coefficient (β), and nonlinear susceptibility ($\chi^{(3)}$).

The experimentally obtained OA and CA transmittance *Z*-scan curves can be theoretically fitted to estimate the third-order nonlinear optical coefficients of a material. For OA *Z*-scan data, the obtained transmittance curve can be fitted with the equation[66–68]

$$T_{OA}(z) = 1 - \left[\left(\frac{1}{2^{3/2}}\right)\left\{\frac{\beta I L_{eff}}{1 + (x)^2}\right\}\right] \quad (2)$$

Here, β represents the 2PA coefficient, I is the incident laser intensity, and $L_{eff} = \dfrac{1 - e^{-\alpha_0 L}}{\alpha_0}$ (L = sample length). Here, $x = (z/z_r)$, and the Rayleigh length (z_r) signifies the effective sample length as $z_r(\text{mm}) = \dfrac{\pi\omega_0^2}{\lambda}$, where ω_0 (mm) is the beam waist at the focus point. Similarly, the nonlinear refraction phase shift of the material is estimated by fitting the experimentally obtained CA *Z*-scan data using the equation[66–68]

$$T_{CA}(z) = 1 - \left[\frac{4x\Delta\phi}{(x^2+1)(x^2+9)}\right] + \left[\frac{2(x^2+3)\Delta\varphi}{(x^2+1)(x^2+9)}\right] \quad (3)$$

Here, $\Delta\phi$ denotes the nonlinear phase shift, and $\Delta\varphi$ is the nonlinear absorption phase shift, and the nonlinear refractive index n_2 is obtained from the expression

$$n_2 = \frac{\Delta\Phi\lambda}{2\pi I L_{eff}} \quad (4)$$

in which λ is the excitation wavelength. The $(\chi^{(3)})$ value can also be obtained as per the following relationships: $\text{Re}|\chi^{(3)}|(m^2/V^2) = 2c\varepsilon_0 n_0^2 n_2(\text{m}^2\,\text{W}^{-1})$, and $\text{Im}|\chi^{(3)}|(m^2/V^2) = \dfrac{c\varepsilon_0\lambda n_0^2\alpha_2(\text{m W}^{-1})}{2\pi}$.

In the present study, the third-order nonlinear optical properties of porphyrins were characterized using a single

Gaussian beam femtosecond *Z*-scan technique. All the *Z*-scan measurements were performed using an 800 nm femtosecond (120 fs, 84 MHz) laser pulse with varying laser intensities.

Theoretically fitted intensity-dependent OA scan curves of all the porphyrins are shown in Fig. 4. The solid lines in Fig. 4 correspond to the theoretical fit using eqn (2). The OA curves of all samples at various intensities show a dip at the laser beam focal position, which clearly indicates the reverse saturable absorption (RSA) behaviour. The observed RSA behaviour can be attributed to the strong two-photon absorption due to the 800 nm wavelength laser excitation. As the intensity increases, there is a prominent increase in the RSA behaviour of all porphyrin samples. The extracted two-photon absorption coefficients of all the samples from the OA curves are shown in Fig. 5. An increasing trend of the two-photon absorption coefficient (β) was followed for all the porphyrins. However, all samples follow an increasing behaviour; $H_2TPP(NO_2)(CF_3)_2$ has the highest and $NiTPP(NO_2)(CF_3)_2$ has the lowest TPA coefficient. The extracted nonlinear coefficients of all samples are tabulated in Table 3.

The closed aperture (CA) *Z*-scan was performed by varying laser beam intensities in a similar range to open aperture data, and the theoretically fitted CA *Z*-scan data are shown in Fig. 6. The CA *Z*-scans exhibit a peak-valley structure, which indicates the self-defocusing negative nonlinear refraction behaviour of the sample. The nonlinearity of materials could stem from the electronic and non-electronic effects. The negative nonlinearity of materials is basically non-electronic nonlinearity, which is observed due to the thermal effects induced on the sample during light propagation through the medium. The observed negative nonlinear refraction behaviour is a consequence of the cumulative thermal effect, which enhances the thermal nonlinearity of porphyrin beyond its electronic nonlinearity. This effect is particularly evident due to the high-repetition rate laser pulses (84 MHz). The existence of nonlinear absorption and nonlinear refraction is responsible for the asymmetry observed in the CA scans. The experimental CA *Z*-scans are analysed by fitting them using eqn (3), which includes both the term for the nonlinear refraction phase ($\Delta\phi$) and the term for the nonlinear absorption phase ($\Delta\varphi$). The solid lines seen in Fig. 6 correspond to the theoretical fit derived from eqn (3).

The nonlinear refractive indices of all the samples with different input laser intensities calculated using eqn (4) are plotted and shown in Fig. 7. The refractive index also shows an increasing behaviour with the laser intensity for all the samples. The highest negative nonlinear refractive index ($(-)\ 40 \times 10^{-17}\ m^2\ W^{-1}$) was obtained for $H_2TPP(NO_2)(CF_3)_2$ and $NiTPP(NO_2)(CF_3)_2$ had the lowest value ($(-)\ 1 \times 10^{-17}\ m^2\ W^{-1}$).

A relative assessment of the NLO parameters obtained in this study is conducted regarding those reported in the literature under picosecond (ps), nanosecond (ns), and femtosecond (fs) laser excitation conditions. Table 4 outlines the NLO parameters documented in the literature for porphyrins and related molecules. Bulbul *et al.*[53,54] studied the third-order nonlinear (NLO) optical properties of highly substituted Ni(II) and *meso*-β monofused porphyrins. By using the *Z*-scan technique with excitation parameters of 800 nm, 120 fs, and

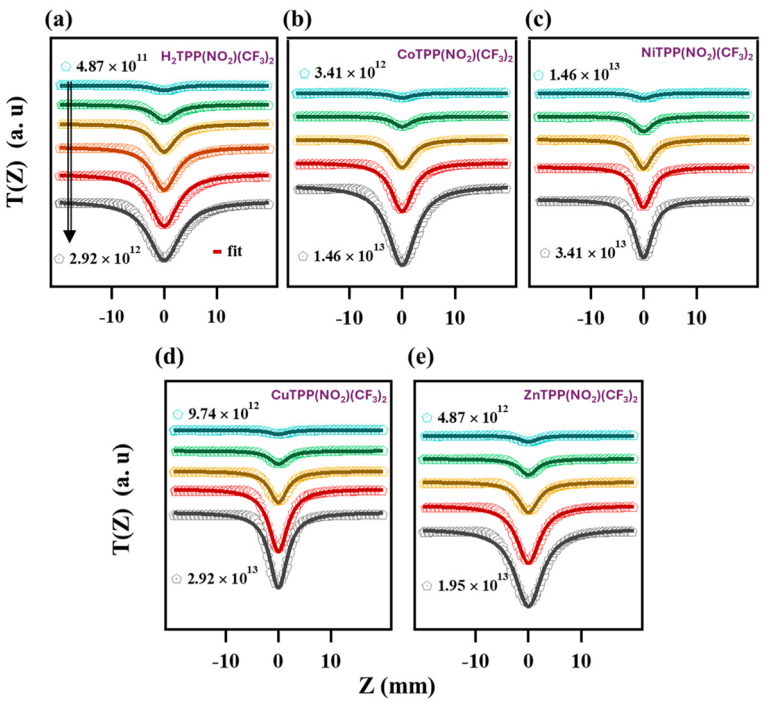

Fig. 4 Intensity-dependent open aperture (OA) experimental *Z*-scan results of (a) $H_2TPP(NO_2)(CF_3)_2$, (b) $CoTPP(NO_2)(CF_3)_2$, (c) $NiTPP(NO_2)(CF_3)_2$, (d) $CuTPP(NO_2)(CF_3)_2$, and (e) $ZnTPP(NO_2)(CF_3)_2$. Laser parameters: 800 nm, 120 fs, and 84 MHz.

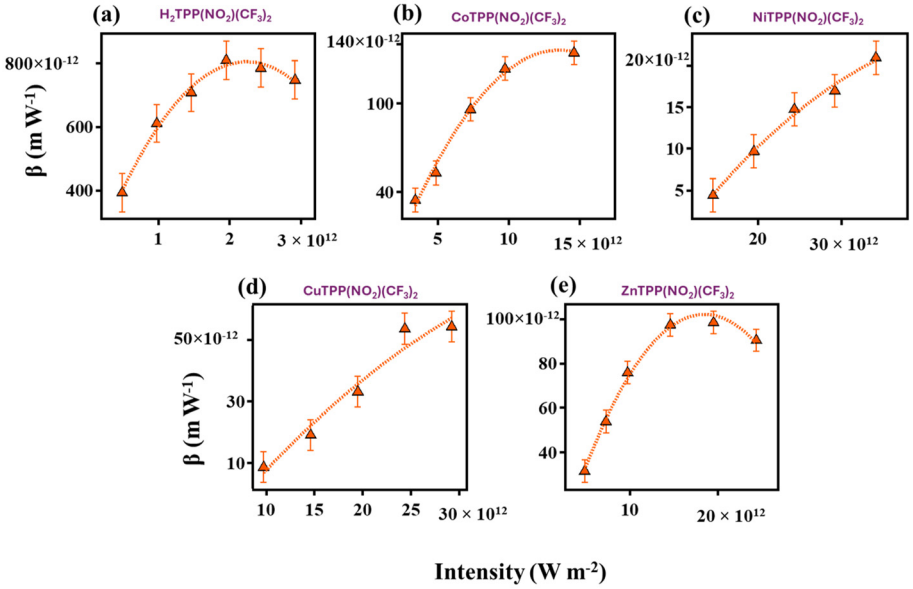

Fig. 5 Nonlinear absorption coefficient (β) extracted from the intensity-dependent open aperture (OA) *Z*-scan results of (a) $H_2TPP(NO_2)(CF_3)_2$, (b) $CoTPP(NO_2)(CF_3)_2$, (c) $NiTPP(NO_2)(CF_3)_2$, (d) $CuTPP(NO_2)(CF_3)_2$ and (e) $ZnTPP(NO_2)(CF_3)_2$. Laser parameters: 800 nm, 120 fs, and 84 MHz. Error bars signify the typical experimental/fitting errors.

Table 3 Summary of the third-order nonlinear optical coefficients extracted from *Z*-scan studies of $MTPP(NO_2)(CF_3)_2$ (M = 2H, Co^{II}, Ni^{II}, Cu^{II}, and Zn^{II}) porphyrins

Intensity (W m^{-2}) (10^{12})	β (m W^{-1}) ($\times 10^{-10}$)	Nonlinear refraction phase ($\Delta\phi$)	Nonlinear absorption phase ($\Delta\varphi$)	σ_{2PA} (GM) ($\times 10^{6}$)	n_2 (m^2 W^{-1}) ($\times 10^{-17}$)	Real $[\chi^{(3)}]$ (esu) ($\times 10^{-11}$)	Im $[\chi^{(3)}]$ (esu) ($\times 10^{-12}$)	Total $[\chi^{(3)}]$ (esu) ($\times 10^{-11}$)
$H_2TPP(NO_2)(CF_3)_2$								
0.49	3.92	−1.52	0.05	0.81	−40.27	−31.36	19.46	31.43
0.97	6.11	−2.54	0.10	1.30	−33.59	−26.17	30.29	26.35
1.46	7.08	−3.11	0.12	1.46	−27.37	−21.32	35.14	21.61
1.95	8.10	−3.28	0.17	1.67	−21.68	−16.89	40.19	17.36
2.44	7.86	−3.27	0.23	1.62	−17.29	−13.47	38.99	14.03
2.92	7.48	−3.55	0.22	1.54	−15.66	−12.20	37.11	12.75
$CoTPP(NO_2)(CF_3)_2$								
3.41	0.35	−2.04	0.12	0.07	−7.70	−5.99	1.72	6.00
4.87	0.53	−2.62	0.10	0.11	−6.94	−5.40	2.62	5.41
7.30	0.96	−3.13	0.16	0.20	−5.52	−4.29	4.76	4.32
9.74	1.24	−3.21	0.26	0.26	−4.24	−3.30	6.13	3.36
14.60	1.34	−3.78	0.20	0.28	−3.33	−2.59	6.65	2.68
$NiTPP(NO_2)(CF_3)_2$								
14.60	0.04	−1.92	0.20	0.01	−1.69	−1.32	0.22	1.32
19.50	0.10	−2.46	0.26	0.02	−1.62	−1.27	0.48	1.27
24.35	0.15	−2.85	0.23	0.03	−1.50	−1.17	0.73	1.18
29.20	0.17	−2.94	0.24	0.04	−1.30	−1.01	0.84	1.01
34.10	0.21	−2.86	0.38	0.04	−1.08	−0.84	1.04	0.85
$CuTPP(NO_2)(CF_3)_2$								
4.87	—	−1.05	0.08	—	−2.78	−2.17	—	—
9.74	0.09	−1.92	0.19	0.02	−2.54	−1.98	0.43	1.98
14.60	0.19	−2.81	0.16	0.04	−2.48	−1.93	0.95	1.93
19.50	0.33	−2.95	0.31	0.07	−1.94	−1.51	1.65	1.52
24.35	0.54	−3.00	0.30	0.11	−1.59	−1.24	2.67	1.26
29.20	0.54	—	—	0.11	—	—	2.70	—
$ZnTPP(NO_2)(CF_3)_2$								
3.41	—	−1.64	0.06	—	−6.17	−4.81	—	—
4.87	0.32	−2.19	0.15	0.06	−5.79	−4.51	1.56	4.51
7.30	0.54	−2.83	0.16	0.11	−4.99	−3.89	2.68	3.90
9.74	0.76	−2.99	0.22	0.16	−3.96	−3.08	3.76	3.11
14.60	0.97	−3.07	0.31	0.20	−2.71	−2.11	4.83	2.16
19.50	0.98	—	—	0.20	—	—	4.89	—

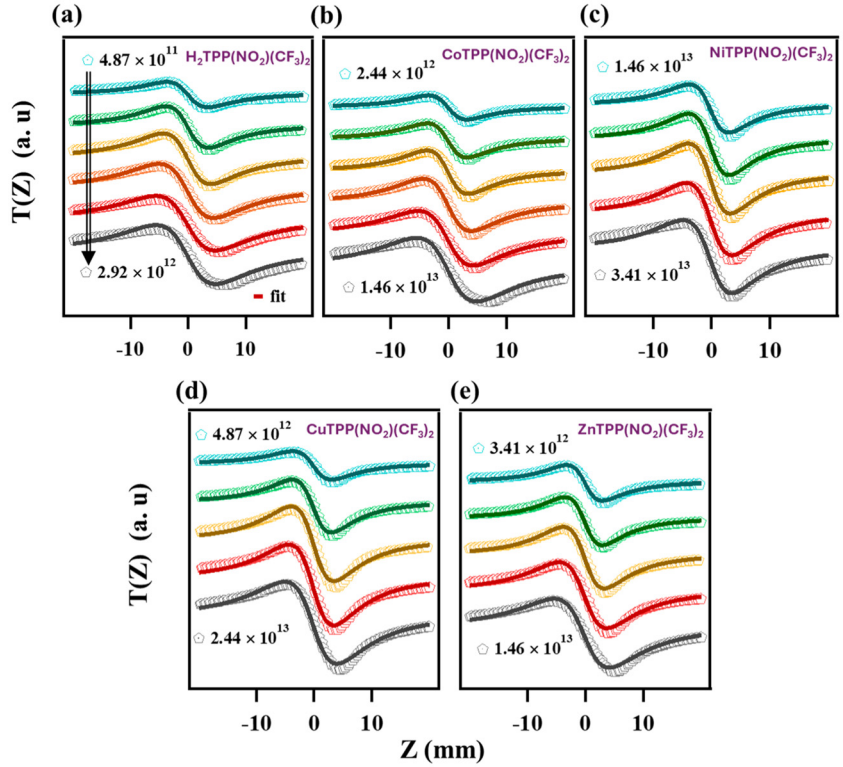

Fig. 6 Intensity-dependent closed aperture (CA) experimental *Z*-scan results of (a) $H_2TPP(NO_2)(CF_3)_2$, (b) $CoTPP(NO_2)(CF_3)_2$, (c) $NiTPP(NO_2)(CF_3)_2$, (d) $CuTPP(NO_2)(CF_3)_2$ and (e) $ZnTPP(NO_2)(CF_3)_2$. Laser parameters: 800 nm, 120 fs, and 84 MHz.

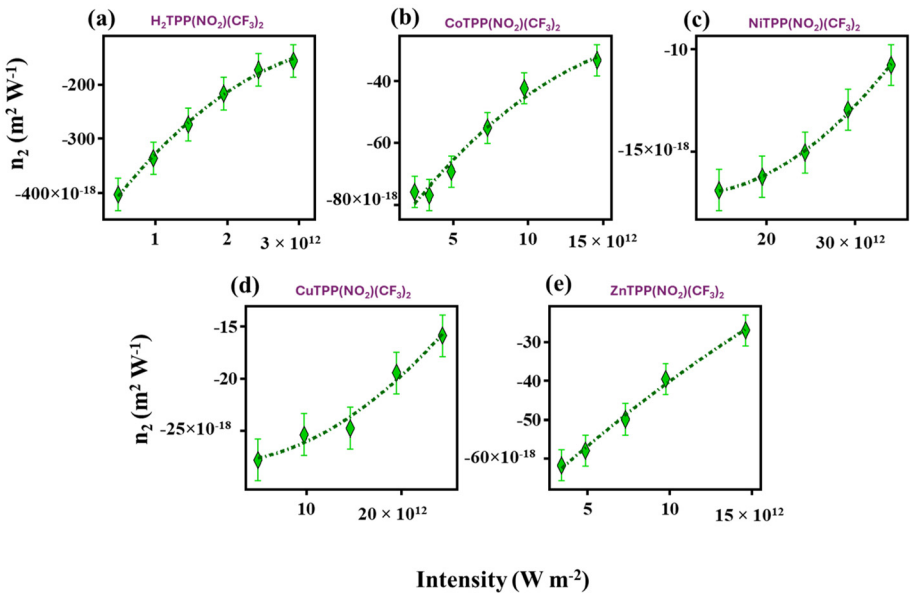

Fig. 7 Nonlinear refractive index (n_2) extracted from the intensity-dependent closed aperture (CA) *Z*-scan results of (a) $H_2TPP(NO_2)(CF_3)_2$, (b) $CoTPP(NO_2)(CF_3)_2$, (c) $NiTPP(NO_2)(CF_3)_2$, (d) $CuTPP(NO_2)(CF_3)_2$ and (e) $ZnTPP(NO_2)(CF_3)_2$. Laser parameters: 800 nm, 120 fs, and 84 MHz. Error bars signify the typical experimental/fitting errors.

84 MHz, they successfully extracted the two-photon absorption coefficient ranges and the nonlinear refractive index ranges as tabulated in Table 4. Bao *et al.*[69] studied the third-order NLO properties of asymmetric and symmetric porphyrin derivatives with excitation parameters 532 nm, 7 ns, and 10 Hz, and their results showed that the two-photon absorption coefficient

Table 4 Summary of NLO data extracted from other porphyrins and related molecules

Porphyrins and their analogs	Laser details	β	n_2	Total $[\chi^{(3)}]$ (esu)	Ref.
MTPP$(NO_2)(CF_3)_2$	800 nm, 120 fs, 84 MHz	0.04–8.10 × 10^{-10} m W^{-1}	(−) 1.08–40.27 × 10^{-17} m^2 W^{-1}	0.85–31.43 × 10^{-11}	This work
meso-β monofused porphyrins	800 nm, 120 fs, 84 MHz	0.18–39.06 × 10^{-11} m W^{-1}	(−) 0.5–5.28 × 10^{-16} m^2 W^{-1}	0.39–2.84 × 10^{-10}	54
Highly substituted Ni(II) porphyrins	800 nm, 120 fs, 84 MHz	22–33 × 10^{-10} m W^{-1}	(−) 4.14–16.30 × 10^{-15} m^2 W^{-1}	3.22–12.69 × 10^{-9}	53
Asymmetric and symmetric porphyrin	532 nm, 7 ns, 10 Hz	0.9–3.7 × 10^{-9} m W^{-1}	(−) 13.0–58.1 × 10^{-10} (esu)	4.2–17.9 × 10^{-11}	69
2D metal-pyridylporphyrinic framework films	532 nm	5.1–57 × 10^{-7} m W^{-1}	(−) 6.5–92 × 10^{-14} m^2 W^{-1}	3.91–54.3 × 10^{-8}	70
trans-A_2B-corroles in solution	1064 nm, 250 fs, 80 MHz	1.9–17.2 × 10^{-15} m W^{-1}	(−) 7.8–25.9 × 10^{-18} m^2 W^{-1}		71
trans-A_2B-corroles in the aggregated state	1064 nm, 250 fs, 80 MHz	2.0–444 × 10^{-13} m W^{-1}	(−) 1.1–71.8 × 10^{-18} m^2 W^{-1}		71
trans-A_2B-type cobalt corroles	532 nm, 4 ns, 10 Hz	1.05–1.45 × 10^{-11} m W^{-1}	(−) 4.46–5.11 × 10^{-11} (esu)	6.46–7.75 × 10^{-12}	72
Push–pull *trans*-A_2B-corroles	800 nm, 150 fs, 80 MHz	0.65–6.80 × 10^{-10} m W^{-1}	(−) 1.30–10.0 × 10^{-10} (esu)	0.31–2.40 × 10^{-9}	44
Zinc porphyrin	532 nm, 3 ns, 10 Hz	1.03–2.08 × 10^{-9} m W^{-1}	(−) 0.77–2.45 × 10^{-9} (esu)		35
Porphyrin-based polyimides	532 nm, 6 ns, 10 Hz	0.51–1.39 × 10^{-5} (esu)	(−) 2.42 –10.26 × 10^{-10} (esu)	3.74–15.65 × 10^{-11}	73
Porphyrin and polyoxometalate hybrids	532 nm, 6 ns, 10 Hz	0.65–2.53 × 10^{-5} (esu)	(−) 0.80–1.56 × 10^{-9} (esu)	1.55–2.38 × 10^{-10}	74
Polyoxometalate–porphyrin hybrids	532 nm, 6 ns, 10 Hz	0.39–2.16 × 10^{-5} (esu)	(−) 0.54–1.65 × 10^{-9} (esu)	0.82–2.52 × 10^{-10}	75
Keggin-type anions and porphyrins	532 nm, 6 ns, 10 Hz	2.08–15.58 × 10^{-6} (esu)	(−) 1.86–12.45 × 10^{-10} (esu)	0.27–1.85 × 10^{-10}	13
Zinc porphyrin and zinc phthalocyanine	680–1080 nm, 150 fs, 80 MHz		(−) 0.5–9.0 × 10^{-15} m^2 W^{-1}	0.06–7.7 × 10^{-9}	11
Porphyrin-POM composite films	532 nm, 7 ns, 10 Hz	0.05–0.45 × 10^{-5} (esu)	(−) 0.12–2.12 × 10^{-10} (esu)	0.30–2.78 × 10^{-11}	76
Porphyrin and polyoxometalate	532 nm, 7 ns, 10 Hz	1.31–1.50 × 10^{-5} (esu)	(−) 1.74–2.22 × 10^{-10} (esu)	3.35–4.15 × 10^{-11}	77
Porphyrin–Anderson type	532 nm, 6 ns, 10 Hz	0.23–14.84 × 10^{-5} (esu)	(−) 1.34–16.80 × 10^{-10} (esu)	2.05–31.72 × 10^{-11}	7
Polyoxometalate hybrid					

ranges from 0.9 to 3.7 × 10^{-9} m W^{-1} and the nonlinear refractive index ranges from (−) 13.0 to 58.1 × 10^{-10} (esu). Li *et al.*[70] documented 2D metal–pyridylporphyrinic framework films and explored their third-order NLO properties using a nanosecond region at a wavelength of 532 nm. They revealed good β and n_2 values ranging from 5.1 to 57 × 10^{-7} m W^{-1} and (−) 6.5 to 92 × 10^{-14} m^2 W^{-1}, respectively. Yasin *et al.*[35] designed π-expanded zinc porphyrins and explored their NLO properties by using 532 nm, 3 ns, and 10 Hz laser parameters. Their findings demonstrated β values ranging from 1.03 to 2.08 × 10^{-9} m W^{-1} and n_2 values ranging from (−) 0.77 to 2.45 × 10^{-9} (esu). Garai *et al.*[71] examined the NLO properties of *trans*-A_2B-corroles in solution and aggregated states using 1064 nm, 250 fs, and 80 MHz laser parameters. Their results revealed that *trans*-A_2B-corroles in an aggregated state showed higher β and n_2 value ranges of 2.0–444 × 10^{-13} m W^{-1} and (−) 1.1–71.8 × 10^{-18} m^2 W^{-1}, respectively, compared to the *trans*-A_2B-corroles in the solution state (β = 1.9–17.2 × 10^{-15} m W^{-1} and n_2 = (−) 7.8–25.9 × 10^{-18} m^2 W^{-1}). Yadav *et al.*[44] investigated push–pull *trans*-A_2B-corroles and assessed their femtosecond third-order NLO properties using excitation parameters of 800 nm, 150 fs, and 80 MHz. Their findings demonstrated that the investigated corroles showed a negative type of nonlinearity and self-defocusing behaviour with the n_2 value ranging from (−) 1.30 to 10.0 × 10^{-10} (esu). In comparison, the asymmetric β-trisubstituted electron-deficient synthesized porphyrins explored in the present study exhibited excellent NLO properties, comparable to the coefficients reported for porphyrins and related molecules in the literature. However, a few studies reported by other groups show one or two orders of magnitude higher than those found in this study.

Conclusions

A series of electron-deficient β-trisubstituted porphyrins $H_2TPP(NO_2)(CF_3)_2$ and their metal complexes MTPP$(NO_2)(CF_3)_2$ (M = Co^{II}, Ni^{II}, Cu^{II} and Zn^{II}) have been synthesized in good yields and characterized spectroscopically and structurally. Single crystal X-ray analysis and DFT optimizations showed the *saddle*-shaped configuration of CoTPP$(NO_2)(CF_3)_2$, NiTPP$(NO_2)(CF_3)_2$ and CuTPP$(NO_2)(CF_3)_2$. The synthesized MTPP$(NO_2)(CF_3)_2$ exhibit a bathochromic shift in the Soret band and longest Q-band ($Q_x(0,0)$) compared to their MTPPs, MTPP(NO_2) and MTPP$(NO_2)Br_2$, which can be attributed to the strong electron-accepting effect of trifluoromethyl groups functionalized at the β-position and the nonplanar conformation of the synthesized porphyrins, demonstrated by the DFT calculations. The considerable downfield shift of NH resonance indicates the electronic effect of substituents and the synthesized porphyrins' nonplanarity compared to H_2TPP, $H_2TPP(NO_2)$, and $H_2TPP(NO_2)Br_2$. The first reduction potential of the synthesized porphyrins reveals that they are easier to reduce compared to similar reported macrocycles. A remarkable reduction in the HOMO–LUMO energy gap of 0.72 V, 0.43 V, and 0.36 V was observed in $H_2TPP(NO_2)(CF_3)_2$ (1.51 V) com-

pared to H_2TPP (2.23 V), $H_2TPP(NO_2)$ (1.97 V) and $H_2TPP(NO_2)Br_2$ (1.87 V), respectively. The synthesized porphyrins showed high ground state dipole moments ranging from 6.42 to 7.75 Debye. The nonlinear optical properties of the synthesized porphyrins were investigated in the visible region (800 nm) using a femtosecond *Z*-scan technique (120 fs, 84 MHz). $H_2TPP(NO_2)(CF_3)_2$ exhibits the highest two-photon absorption coefficient (β) and cross-section (σ_{2PA}) among all the studied compounds, 8.10×10^{-10} m W^{-1} and 1.67×10^6 GM, respectively. These results suggest that the synthesized porphyrins hold the potential for advanced applications in photonic devices and other optoelectronic technologies.

Data availability

Data are available in the submitted article's ESI.†

Conflicts of interest

The authors declare no conflict of interest.

Acknowledgements

The authors gratefully acknowledge the Science and Engineering Research Board (SERB/CRG/2020/005958) for financial support. Reena Jangra thanks the Ministry of Education (MoE), Govt. of India, for the senior research fellowship. The authors thank DST-FIST, New Delhi, for providing funds (SR/FST/CS-II/2018/72(C)) to purchase 500 MHz NMR and SCXRD instruments.

References

1 Z. B. Qin, Y. Q. Wen, Y. L. Shang, Y. L. Song and Y. Z. Wan, *Appl. Phys. A:Mater. Sci. Process.*, 2007, **87**, 277–280.
2 F. Castet, V. Rodriguez, J. L. Pozzo, L. Ducasse, A. Plaquet and B. Champagne, *Acc. Chem. Res.*, 2013, **46**, 2656–2665.
3 R. Bano, M. Asghar, K. Ayub, T. Mahmood, J. Iqbal, S. Tabassum, R. Zakaria and M. A. Gilani, *Front. Mater.*, 2021, **8**, 1–24.
4 X. Han, L. Ding, Z. Tian, Y. Song, R. Xiong, C. Zhang, J. Han and S. Jiang, *Int. J. Biol. Macromol.*, 2023, **224**, 1236–1243.
5 K. Senthil, S. Kalainathan, A. R. Kumar and P. G. Aravindan, *RSC Adv.*, 2014, **4**, 56112–56127.
6 M. O. Senge, M. Fazekas, E. G. A. Notaras, W. J. Blau, M. Zawadzka, O. B. Locos and E. M. N. Mhuircheartaigh, *Adv. Mater.*, 2007, **19**, 2737–2774.
7 S. Ul Hassan, H. M. Asif, Y. Zhou, L. Zhang, N. Qu, J. Li and Z. Shi, *J. Phys. Chem. C*, 2016, **120**, 27587–27599.
8 B. Champagne, A. Plaquet, J. L. Pozzo, V. Rodriguez and F. Castet, *J. Am. Chem. Soc.*, 2012, **134**, 8101–8103.
9 B. P. Biswal, S. Valligatla, M. Wang, T. Banerjee, N. A. Saad, B. M. K. Mariserla, N. Chandrasekhar, D. Becker, M. Addicoat, I. Senkovska, R. Berger, D. N. Rao, S. Kaskel and X. Feng, *Angew. Chem., Int. Ed.*, 2019, **58**, 6896–6900.
10 Y. Zhai, J. Q. Yang, Y. Zhou, J. Y. Mao, Y. Ren, V. A. L. Roy and S. T. Han, *Mater. Horiz.*, 2018, **5**, 641–654.
11 M. S. S. Bharati, S. Bhattacharya, J. V. S. Krishna, L. Giribabu and S. V. Rao, *Opt. Laser Technol.*, 2018, **108**, 418–425.
12 M. Samal, S. Valligatla, N. A. Saad, M. V. Rao, D. N. Rao, R. Sahu and B. P. Biswal, *Chem. Commun.*, 2019, **55**, 11025–11028.
13 F. Khurum Shehzad, A. Iqbal, Y. Zhou, L. Zhang, T. Wang and X. Ren, *J. Phys. Chem. C*, 2020, **124**, 9442–9450.
14 K. Kandasamy, S. J. Shetty, P. N. Puntambekar, T. S. Srivastava, T. Kundu and B. P. Singh, *J. Porphyrins Phthalocyanines*, 1999, **3**, 81–86.
15 W. Blau, H. Byrne, W. M. Dennis and J. M. Kelly, *Opt. Commun.*, 1985, **56**, 25–29.
16 C. Ryppa, D. Niedzwiedzki, N. L. Morozowich, R. Srikanth, M. Zeller, H. A. Frank and C. Bruckner, *Chem. – Eur. J.*, 2009, **15**, 5749–5762.
17 J. Humphrey and D. Kuciauskas, *J. Phys. Chem. B*, 2004, **108**, 12016–12023.
18 P. P. Kiran, D. R. Reddy, B. G. Maiya, A. K. Dharmadhikari, G. R. Kumar and D. N. Rao, *Opt. Commun.*, 2005, **252**, 150–161.
19 J. E. Reeve, H. A. Collins, K. De Mey, M. M. Kohl, K. J. Thorley, O. Paulsen, K. Clays and H. L. Anderson, *J. Am. Chem. Soc.*, 2009, **131**, 2758–2759.
20 T. Zhang, Y. Zhao, K. Song, I. Asselberghs, A. Persoons, K. Clays and M. J. Therien, *Inorg. Chem.*, 2006, **45**, 9703–9712.
21 X. Hu, D. Xiao, S. Keinan, I. Asselberghs, M. J. Therien, K. Clays, W. Yang and D. N. Beratan, *J. Phys. Chem. C*, 2010, **114**, 2349–2359.
22 H. L. Anderson, *Adv. Mater.*, 1994, **6**, 834–836.
23 H. L. Anderson, S. J. Martin and D. D. C. Bradley, *Angew. Chem., Int. Ed. Engl.*, 1994, **33**, 655–657.
24 T. E. O. Screen, J. R. G. Thorne, R. G. Denning, D. G. Bucknall and H. L. Anderson, *J. Mater. Chem.*, 2003, **13**, 2796–2808.
25 P. N. Taylor, A. P. Wylie, J. Huuskonen and H. L. Anderson, *Angew. Chem., Int. Ed.*, 1998, **37**, 986–989.
26 J. R. G. Thorne, S. M. Kuebler, R. G. Denning, I. M. Blake, P. N. Taylor and H. L. Anderson, *Chem. Phys.*, 1999, **248**, 181–193.
27 J. L. Sessler and D. Seidel, *Angew. Chem., Int. Ed.*, 2003, **42**, 5134–5175.
28 Z. S. Yoon, J. H. Kwon, M. C. Yoon, M. K. Koh, S. B. Noh, J. L. Sessler, J. T. Lee, D. Seidel, A. Aguilar, S. Shimizu, M. Suzuki, A. Osuka and D. Kim, *J. Am. Chem. Soc.*, 2006, **128**, 14128–14134.
29 A. Tsuda, A. Nakano, H. Furuta, H. Yamochi and A. Osuka, *Angew. Chem., Int. Ed.*, 2000, **39**, 558–561.

30 I. V. Rubtsov, K. Susumu, G. I. Rubtsov and M. J. Therien, *J. Am. Chem. Soc.*, 2003, **125**, 2687–2696.
31 Y. Matsuzaki, A. Nogami, A. Tsuda, A. Osuka and K. Tanaka, *J. Phys. Chem. A*, 2006, **110**, 4888–4899.
32 Y. Matsuzaki, A. Nogami, Y. Iwaki, N. Ohta, N. Yoshida, N. Aratani, A. Osuka and K. Tanaka, *J. Phys. Chem. A*, 2005, **109**, 703–713.
33 Z. B. Liu, Y. F. Xu, X. Y. Zhang, X. L. Zhang, Y. S. Chen and J. G. Tian, *J. Phys. Chem. B*, 2009, **113**, 9681–9686.
34 R. Jangra and M. Sankar, *J. Porphyrins Phthalocyanines*, 2025, **29**, 123–133.
35 A. Yasin, V. S. Nair, M. H. Ab Rahim, Y. Yamaoka, C. S. Yelleswarapu and R. Jose, *J. Mater. Chem. C*, 2021, **9**, 17461–17470.
36 K. S. Suslick, C. Chen, G. R. Meredith and L.-T. Cheng, *J. Am. Chem. Soc.*, 1992, **114**, 6928–6930.
37 T. Morotti, M. Pizzotti, R. Ugo, S. Quici, M. Bruschi, P. Mussini and S. Righetto, *Eur. J. Inorg. Chem.*, 2006, 1743–1757.
38 K. J. McEwan, G. Bourhill, J. M. Robertson and H. L. Anderson, *J. Nonlinear Opt. Phys. Mater.*, 2000, **9**, 451–468.
39 P. T. Anusha, A. R. Thomas, R. Philip and S. V. Rao, *Chem. Phys. Lett.*, 2015, **641**, 23–28.
40 P. Liang, Y. Mi, J. Duan, Z. Yang, D. Wang, H. Cao, W. He and H. Yang, *Chin. J. Chem.*, 2016, **34**, 381–386.
41 T. Tanaka and A. Osuka, *Chem. Soc. Rev.*, 2015, **44**, 943–969.
42 S. M. LeCours, H. W. Guan, S. G. DiMagno, C. H. Wang and M. J. Therien, *J. Am. Chem. Soc.*, 1996, **118**, 1497–1503.
43 C. C. Yang, L. Li, W. Q. Tian, W. Q. Li and L. Yang, *Phys. Chem. Chem. Phys.*, 2022, **24**, 13275–13285.
44 P. Yadav, T. Anand, S. S. B. Moram, S. Bhattacharya, M. Sankar and S. V. Rao, *Dyes Pigm.*, 2017, **143**, 324–330.
45 P. Rathi, Ekta, S. Kumar, D. Banerjee, V. R. Soma and M. Sankar, *Dalton Trans.*, 2020, **49**, 3198–3208.
46 S. Kumar, J. N. Acharyya, D. Banerjee, V. R. Soma, G. V. Prakash and M. Sankar, *Dalton Trans.*, 2021, **50**, 6256–6272.
47 R. K. Rohal, M. Shanu, J. N. Acharyya, G. V. Prakash and M. Sankar, *Dalton Trans.*, 2022, **51**, 9049–9061.
48 R. K. Rohal, J. N. Acharyya, M. Shanu, G. V. Prakash and M. Sankar, *Inorg. Chem.*, 2022, **61**, 1297–1307.
49 A. S. Bulbul, N. Chaudhri, M. Shanu, J. N. Acharyya, G. V. Prakash and M. Sankar, *Inorg. Chem.*, 2022, **61**, 9968–9982.
50 I. Yadav, M. Shanu, J. N. Acharyya, G. V. Prakash and M. Sankar, *Inorg. Chem.*, 2022, **61**, 19289–19301.
51 S. Kumari, I. Yadav, J. N. Acharyya, M. Shanu, G. V. Prakash and M. Sankar, *Dyes Pigm.*, 2023, **217**, 111416.
52 R. K. Rohal, D. Banerjee, N. Rana, V. R. Soma and M. Sankar, *Dalton Trans.*, 2024, **53**, 6436–6444.
53 A. S. Bulbul, A. Kuriakose, R. Komal, J. N. Acharyya, G. V. Prakash and M. Sankar, *Inorg. Chem.*, 2024, **63**, 17967–17982.
54 A. S. Bulbul, R. Jangra, A. Kuriakose, N. J. Acharyya, G. V. Prakash and M. Sankar, *Chem. – Eur. J.*, 2025, e202403473.
55 A. S. Bulbul, J. Mogilipuri, V. R. Soma and M. Sankar, *Dalton Trans.*, 2025, **54**, 3679–3694.
56 R. Kumar and M. Sankar, *Inorg. Chem.*, 2014, **53**, 12706–12719.
57 W. Arif and R. Kumar, *ChemistrySelect*, 2023, **8**, e202304575.
58 Z. Zhou, Q. Liu, Z. Yan, G. Long, X. Zhang, C. Cao and R. Jiang, *Org. Lett.*, 2013, **15**, 606–609.
59 A. B. J. Parusel, T. Wondimagegn and A. Ghosh, *J. Am. Chem. Soc.*, 2000, **122**, 6371–6374.
60 S. G. DiMagno, A. K. Wertsching and C. R. Ross, *J. Am. Chem. Soc.*, 1995, **117**, 8279–8280.
61 A. G. Mojarrad and S. Zakavi, *RSC Adv.*, 2016, **6**, 100931–100938.
62 V. V. Smirnov, E. K. Woller and S. G. DiMagno, *Inorg. Chem.*, 1998, **37**, 4971–4978.
63 C. J. Medforth and J. J. Smith, *Tetrahedron Lett.*, 1990, **31**, 5583–5586.
64 K. M. Kadish, X. Q. Lin and B. C. Han, *Inorg. Chem.*, 1987, **26**, 4161–4167.
65 K. M. Kadish, Z. Ou, X. Tan, T. Boschi, D. Monti, V. Fares and P. Tagliatesta, *Dalton Trans.*, 1999, **25**, 1595–1601.
66 M. Sheik-Bahae, A. A. Said, T. H. Wei, D. J. Hagan and E. W. Van Stryland, *IEEE J. Quantum Electron.*, 1990, **26**, 760–769.
67 J. N. Acharyya, D. N. Rao, M. Adnan, C. Raghavendar, R. B. Gangineni and G. V. Prakash, *Adv. Mater. Interfaces*, 2020, **7**, 2000035.
68 M. Priyadarshini, J. N. Acharyya, S. Mahajan and G. V. Prakash, *Opt. Laser Technol.*, 2021, **139**, 107008.
69 C. Bao, Y. Li, Y. Li, Z. Si, Y. Zhang, C. Chen, L. Wang and Q. Duan, *New J. Chem.*, 2021, **45**, 16030–16038.
70 D. J. Li, Q. H. Li, Z. G. Gu and J. Zhang, *Nano Lett.*, 2021, **21**, 10012–10018.
71 A. Garai, S. Kumar, W. Sinha, C. S. Purohit, R. Das and S. Kar, *RSC Adv.*, 2015, **5**, 28643–28651.
72 G. Lu, P. Zhang, Y. Fang, Y. Gao and Q. Hu, *New J. Chem.*, 2021, **45**, 2103–2109.
73 F. K. Shehzad, Q. U. Khan, Q. Mahmood, F. Ghafoor, H. O. Alsaab, S. A. A. Shah, N. Athir and A. Iqbal, *Opt. Mater.*, 2022, **127**, 112317.
74 T. Akhtar, U. Saleem, H. K. Thabet, F. K. Shehzad, K. Mehmood, A. Iqbal, H. M. Asif, Z. M. El-Bahy, H. I. A. Qazi and M. Sohail, *Spectrochim. Acta, Part A*, 2024, **319**, 124551.
75 H. M. Asif, A. Iqbal, Y. Zhou, L. Zhang, T. Wang, M. I. U. Farooqi and R. Sun, *Dyes Pigm.*, 2021, **184**, 108758.
76 Z. Shi, Y. Zhou, L. Zhang, D. Yang, C. Mu, H. Ren, F. K. Shehzad and J. Li, *Dalton Trans.*, 2015, **44**, 4102–4107.
77 Z. Shi, Y. Zhou, L. Zhang, C. Mu, H. Ren, D. U. Hassan, D. Yang and H. M. Asif, *RSC Adv.*, 2014, **4**, 50277–50284.